PLANT SCIENCES

The polymerase-associated factor 1 complex modulates the growth-defense tradeoff in *Arabidopsis*

Yuyu Guo[1,2,3,4,5]†, Cunliang Li[1,2,3,4,5]†, Yao Liu[1,2,3,4,5], Hanyi Mao[1,2,3,4,5], Yin Zhang[1,2,3,4,5], Pascal Genschik[6], Lili Wang[1,2,3,4,5], Shunping Yan[1,2,3,4,5]*

Plants have evolved sophisticated mechanisms to balance growth and defense. The evolutionarily conserved polymerase-associated factor 1 complex (PAF1C) plays multiple roles in transcription. Here, we show that PAF1C regulates the growth-defense tradeoff by repressing defense genes expression in *Arabidopsis*. Loss of PAF1C leads to increased expression of defense genes, enhanced disease resistance, but compromised growth. Mechanistically, PAF1C binds to defense genes, where it interacts with histone deacetylases, such as HDA6, to promote histone deacetylation, thereby repressing defense genes expression. The plant immune hormone salicylic acid (SA) promotes the interaction between PAF1 and the SA receptor NPR1, which functions as an E3 ubiquitin ligase to mediate the polyubiquitination and degradation of PAF1. Genetically, loss of PAF1 suppresses the immune defects of the *npr1* mutant, supporting the notion that PAF1 functions downstream of NPR1. Collectively, this study identifies the NPR1-PAF1C-HDA6 module that regulates the growth-defense tradeoff.

INTRODUCTION

Plants are frequently attacked by various types of pathogens, including bacteria, fungi, oomycetes, and viruses (*1*, *2*). To defend against pathogens, plants have evolved complex and elaborate disease resistance mechanisms including pattern-triggered immunity, effector-triggered immunity, and systemic acquired resistance (*3*, *4*). Disease resistance mechanisms prevent or limit pathogen infection and growth and thus are energy-consuming processes, often causing reduced growth, which is called the growth-defense tradeoff (*5*–*8*). Therefore, disease resistance mechanisms must be tightly controlled to ensure efficient activation in the presence of pathogens and kept inactive in the absence of pathogens. Unlike disease resistance mechanisms, plant disease tolerance mechanisms are distinct immune strategies for maintaining plant health by alleviating the host fitness costs from pathogens without limiting infection and thus attract more and more attentions (*9*–*12*).

Salicylic acid (SA) is one of the most important plant immune hormones (*13*). Upon pathogen infection, plants synthesize more SA and thus induce the expression of genes involved in immune responses (*14*–*16*). Through genetic and biochemical studies, nonexpresser of PR genes 1 (NPR1), and its paralogs NPR3/4 were identified as SA receptors (*17*–*21*). Basically, NPR1/3/4 function through two mechanisms. On one hand, they function as transcriptional coregulators by interacting with transcription factors such as TGACG motif-binding factors (TGAs) (*22*, *23*). While NPR1 promotes gene expression, NPR3/4 inhibit gene expression (*17*, *24*). On the other hand, they function as ubiquitin E3 ligases by interacting with Cullin 3 (*25*–*28*). Compared with their functions in transcription, their roles in ubiquitination are far less well-understood. NPR3/4 has been shown to ubiquitinate NPR1 and promotes its degradation (*19*). Recently, it was reported that NPR1 mediates the ubiquitination and degradation of immune regulators including EDS1, NIMIN1, WRKY54, and WRKY70 (*27*). Previously, we found that NPR1 mediates the ubiquitination and degradation of the gibberellin receptor GA insensitive dwarf 1 (GID1) to inhibit plant growth (*29*).

The polymerase-associated factor 1 (PAF1) complex (PAF1C) is evolutionarily conserved in eukaryotes (*30*, *31*). The *Arabidopsis* PAF1C contains six subunits, namely, PAF1, VIP3, VIP4, VIP5, VIP6, and CDC73 (*32*–*36*). The most well-studied function of PAF1 is to regulate gene expression by interacting with RNA polymerase II (RNA Pol II) (*37*, *38*). For example, PAF1C can promote the expression of *FLC*, which inhibits flowering (*33*, *39*–*41*). Recently, we showed that PAF1C interacts with the SMC5/6 complex to facilitate DNA double-strand break repair in *Arabidopsis* (*42*).

In this study, we found that the *Arabidopsis paf1* mutant showed retarded growth, enhanced expression of immune-related genes, and increased resistance to pathogens. PAF1C binds immune-related genes such as *PATHOGENESIS-RELATED 1* (*PR1*), where PAF1C recruits the histone deacetylases (HDACs) HDA6 to promote H3 deacetylation and thus inhibit gene expression. SA promotes NPR1-mediated polyubiquitination and degradation of PAF1 to derepress immune-related gene expression. In conclusion, our study identified the NPR1-PAF1C-HDA6 module that regulates the growth-defense tradeoff.

RESULTS

Loss of PAF1C enhances disease resistance

In a previous study, we performed a genetic screen for DNA damage response mutant (*DDRM*) in *Arabidopsis* and found that *ddrm4-1*, which contained a T-DNA insertion in the first exon of *PAF1*, was hypersensitive to DNA damage-inducing agents (*42*). We renamed *ddrm4-1* as *paf1-1*. To investigate the role of PAF1 in transcriptional regulation, we carried out RNA sequencing (RNA-seq) analysis, which revealed that 1702 genes were up-regulated and 1920 genes were down-regulated ($|\log_2\text{foldchange}| > 1$, P value < 0.05) in *paf1-1*

[1]Hubei Hongshan Laboratory, Wuhan, 430070, China. [2]College of Life Science and Technology, Huazhong Agricultural University, Wuhan, Hubei 430070, China. [3]Shenzhen Institute of Nutrition and Health, Huazhong Agricultural University, Shenzhen 518000, China. [4]Shenzhen Branch, Guangdong Laboratory for Lingnan Modern Agriculture, Shenzhen 518000, China. [5]Agricultural Genomics Institute at Shenzhen, Chinese Academy of Agricultural Sciences, Shenzhen 518000, China. [6]Institut de Biologie Moléculaire des Plantes, CNRS, Université de Strasbourg, 12, rue du Général Zimmer, Strasbourg 67084, France.
*Corresponding author. Email: spyan@mail.hzau.edu.cn
†These authors contributed equally to this work.

compared to the wild-type Col-0 (Fig. 1A and dataset S1). Gene Ontology (GO) analysis on the up-regulated genes revealed that the immune-related GO terms (e.g., defense response, immune response, response to bacterium, and response to SA) were significantly enriched (Fig. 1B and dataset S2). Among them, some were well-known defense genes such as *PR1*, *EDS5*, *WRKY48*, and *WRKY54*. GO analysis on the down-regulated genes revealed that the growth-related GO terms (e.g., photosynthesis, fatty acid biosynthesis, and organic acid biosynthesis) were significantly enriched (fig. S1 and dataset S3). This result indicated that PAF1 may regulate the growth-defense tradeoff.

Because *PR1* is commonly used as a defense gene marker, we performed reverse transcription–quantitative polymerase chain reaction (RT-qPCR) analysis on *PR1* to verify the RNA-seq results. Consistently, the expression of *PR1* was significantly up-regulated in *paf1-1* and *paf1-2* compared to Col-0 (Fig. 1C and fig. S2A). The enhanced expression of defense genes suggested that the *paf1* mutant may be more resistant to pathogens than Col-0. To test this, we infected *Arabidopsis* leaves with *Pseudomonas syringae* pv. *maculicola* ES4326 (*Psm* ES4326). The disease symptoms of *paf1-1* and *paf1-2* were less severe than those of Col-0 (Fig. 1D and fig. S2B). Consistently, the growth of *Psm* ES4326 was significantly reduced in *paf1-1* and *paf1-2* mutants compared to Col-0 (Fig. 1E and fig. S2C). As a result of enhanced immune responses, the growth of the *paf1-1* and *paf1-2* mutant plants was compromised, as evidenced by the smaller rosette size and reduced fresh weight (fig. S2, S and T). These data suggested that PAF1 negatively regulates plant immune responses to facilitate growth in the absence of pathogens.

PAF1 is the core subunit of PAF1C, which contains PAF1, VIP3, VIP4, VIP5, VIP6, and CDC73 subunits. To determine whether the enhanced disease resistance of *paf1* is attributed to the specific

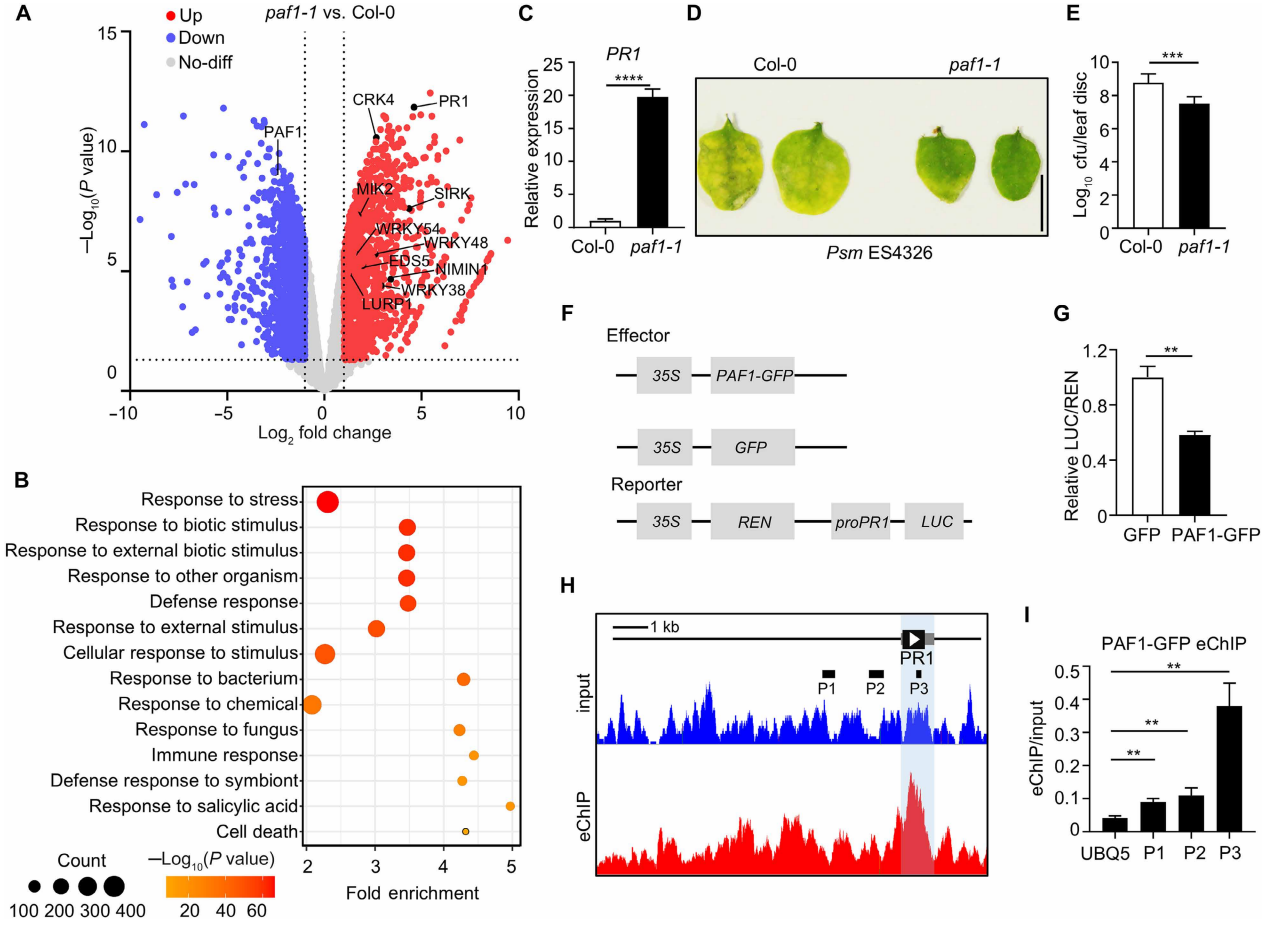

Fig. 1. PAF1 is involved in plant immunity by inhibiting defense genes expression. (**A**) Volcano plot analysis of gene expression in *paf1-1* and Col-0 in RNA-seq assays. Up, up-regulated. Down, down-regulated. No-diff, no difference. (**B**) GO analysis of the up-regulated genes in *paf1-1*. The top 14 significantly enriched GO terms are shown. (**C**) Relative expression of *PR1* determined through RT-qPCR analysis. The data are represented as means ± SD ($n = 3$). (**D**) Representative leaves at 3-days postinfection (dpi) by *Psm* ES4326 [optical density at 600 nm (OD_{600}) = 0.001]. Scale bar, 0.5 cm. (**E**) Growth of *Psm* ES4326 in the leaves at 3 dpi. The data are represented as means ± SD ($n = 8$). (**F**) Schematic representation of the constructs used in the dual-luciferase reporter assays. *35S*, the *35S* promoter; *proPR1*, the *PR1* promoter; LUC, firefly luciferase; REN, renilla luciferase. (**G**) Dual-luciferase reporter assays. The reporter and effector were co-expressed in *Arabidopsis* protoplasts. The relative LUC activities normalized to the REN activities are shown (LUC/REN). The data are represented as means ± SD ($n = 3$). (**H**) eChIP-seq assays. The *35S:PAF1-GFP*/Col-0 seedlings were used for eChIP-seq analysis. The immunoprecipitation was carried out using an α-GFP antibody. Both the immunoprecipitated DNA and the input DNA were subjected to next-generation sequencing analysis. P1, P2, and P3 represent the regions used in the enhanced chromatin immunoprecipitation (eChIP)–quantitative polymerase chain reaction (qPCR) assays. (**I**) eChIP-qPCR assays. The ratios of eChIP and input are shown. *UBQ5* serves as a negative control. The data are represented as means ± SD ($n = 3$). The statistical significance was determined using a two-tailed Student's *t* test. $^{**}P < 0.01$, $^{***}P < 0.001$, and $^{****}P < 0.0001$.

function of PAF1 or the general function of PAF1C, we examined the expression of *PR1* and the resistance to *Psm* ES4326 in other PAF1C mutants. Similar to *paf1*, *vip3-2*, *cdc73-5*, *vip4-c1*, *vip5-2*, and *vip6-c1* showed enhanced *PR1* expression (fig. S2, D, G, J, M, and P), less severe disease symptoms (fig. S2E, H, K, N, and Q), and reduced growth of *Psm* ES4326 (fig. S2, F, I, L, O, and R). The growth of these mutants was also compromised (fig. S2, S and T). Therefore, the whole PAF1C is involved in the growth-defense tradeoff.

PAF1 binds to defense genes and represses their expression

To exclude the possibility that the enhanced defense genes expression in the *paf1* mutant is only indirectly linked to plant growth defects, we examined the role of PAF1 on the transcription of *PR1* using the dual-luciferase reporter assays in *Arabidopsis* protoplasts. The effector constructs contain *GFP* or *PAF1-GFP* driven by the *CaMV* 35*S* promoter (Fig. 1F). The reporter construct contains firefly luciferase (LUC) driven by the *PR1* promoter, and renilla luciferase (REN) driven by the 35*S* promoter. The ratio of LUC to REN represents the activity of *PR1* promoter. Compared with the green fluorescent protein (GFP) control, PAF1-GFP significantly reduced the ratio of LUC and REN (Fig. 1G).

To further confirm the direct role of PAF1 in defense genes expression, we performed enhanced chromatin immunoprecipitation (eChIP) assays using a *35S:PAF1-GFP* transgenic *Arabidopsis* line. Sequencing analysis revealed that PAF1 bound to 6117 genes (dataset S4), among which 561 genes were up-regulated and 395 genes were down-regulated in *paf1-1* (fig. S3A and dataset S5). GO analysis on the 561 up-regulated genes revealed that the immune-related GO terms (e.g., defense response, response to bacterium, and immune system process) were significantly enriched (fig. S3B and dataset S6). As expected, PAF1 bound to *PR1* (Fig. 1H), which was confirmed through eChIP-qPCR analysis (Fig. 1I). Collectively, these data demonstrated that PAF1 binds to defense genes and represses their expression.

PAF1 physically interacts with HDA6

PAF1C is well known to promote gene expression. Therefore, the finding that PAF1C represses defense genes is very interesting. We reasoned that PAF1 may recruit some proteins involved in gene repression. In a previous study, many proteins that copurified with PAF1 were identified (*43*). Among them, several HDACs including HDA19, HDT1, HDT2, HDT3, and HDT4 attracted our attention because HDACs are well-known to repress gene expression (*44*, *45*). Among 18 HDACs in *Arabidopsis*, HDT1, HDT2, HDT3, and HDT4 belong to the plant-specific HD2 family, and HDA19 together with HDA6, HDA7, and HDA9 forms a subfamily in the RPD3/HDA1 super-family (*46*, *47*). To investigate the molecular interactions between PAF1 and HDACs, we performed yeast two-hybrid (Y2H) assays, which revealed that PAF1 could interact with HDA6, HDA7, HDA9, HDA19, and HDT4 (Fig. 2A and fig. S4). Because HDA6

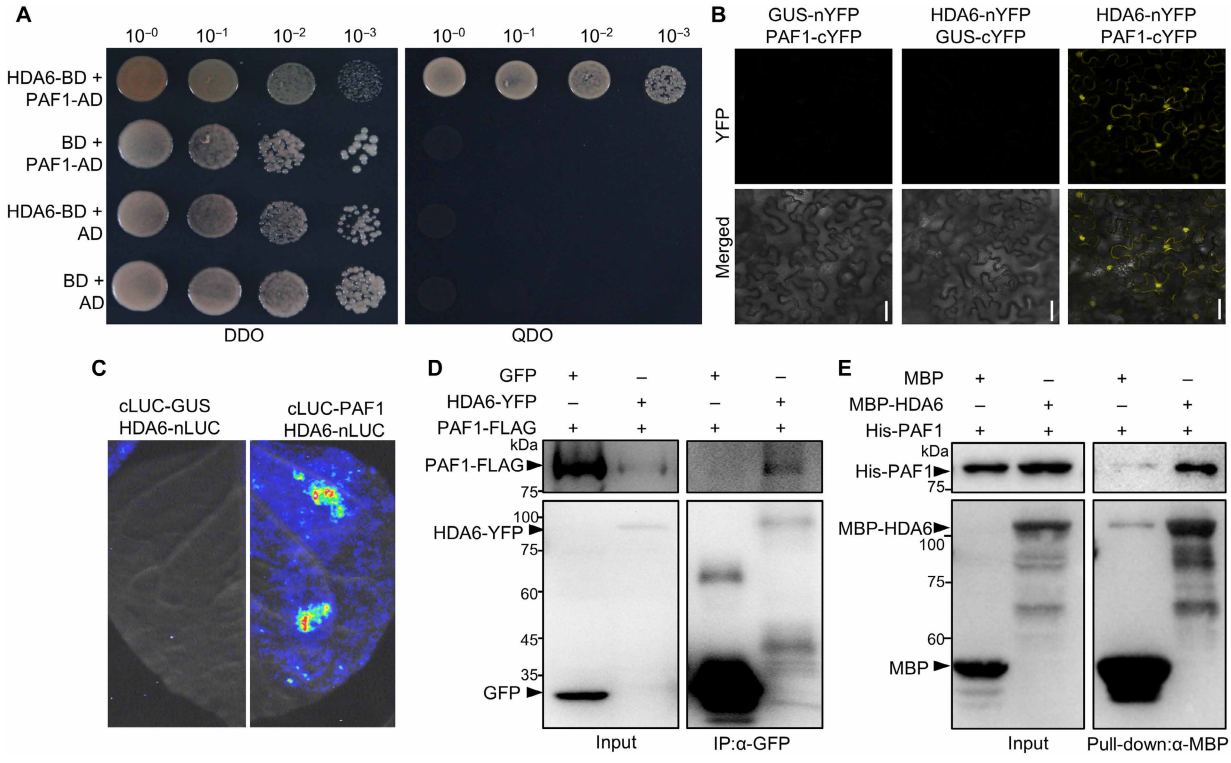

Fig. 2. PAF1 physically interacts with HDA6. (**A**) Y2H assays. AD, activation domain. BD, DNA binding domain. DDO, double dropout (SD/-Trp/-Leu) medium. QDO, quadruple dropout (SD/-Trp/-Leu/-His/-Ade) medium. The yeasts were grown for 4 days. (**B**) BiFC assays. The proteins were fused to either the C- or N-terminal half of YFP (cYFP or nYFP) and were transiently expressed in *N. benthamiana*. GUS serves as a negative control. The YFP fluorescence detected by confocal microscopy indicates interaction. Scale bars, 40 μm. (**C**) Split luciferase assays. The proteins were fused to either the C- or N-terminal half of luciferase (cLUC or nLUC) and were transiently expressed in *N. benthamiana*. The luminescence detected by a charge-coupled device (CCD) camera indicates interaction. (**D**) CoIP assays. PAF1-FLAG was coexpressed with HDA6-YFP or GFP in *N. benthamiana*. The immunoprecipitation was carried out using α-GFP beads. (**E**) Pull-down assays. The MBP or MBP-HDA6 coupled with the dextrin beads were incubated with His-PAF1.

was recently found to repress *PR1* expression (*48*), we focused on HDA6 in the subsequent experiments. We performed bimolecular fluorescence complementation (BiFC) assays (Fig. 2B), split luciferase assays (Fig. 2C), and co-immunoprecipitation (CoIP) assays (Fig. 2D). All these assays revealed that PAF1 interacts with HDA6 in vivo. To test whether the interaction is direct or indirect, we carried out in vitro pull-down assays using purified recombinant proteins. Consistently, His-PAF1 was specifically pulled down by MBP-HDA6, but not the MBP control (Fig. 2E). Therefore, PAF1 directly interacts with HDA6 both in vitro and in vivo.

PAF1 recruits HDA6 to promote H3 deacetylation at defense genes

To test the genetic relationship between PAF1C and HDA6, we generated the *hda6-7 paf1-1* double mutant. Consistent with the previous study (*48*), the expression of *PR1* in *hda6-7* was significantly higher than that in Col-0, mimicking *paf1-1* (Fig. 3A). The expression of *PR1* in *hda6-7 paf1-1* was similar to that in *paf1-1*, indicating that PAF1 and HDA6 function in the same pathway. We also examined the disease resistance of *paf1-1*, *hda6-7*, and *hda6-7 paf1-1* to *Psm* ES4326. The disease symptoms of *paf1-1*, *hda6-7*, and *hda6-7 paf1-1* were less severe than those of Col-0 (Fig. 3B). Consistently, the growth of *Psm* ES4326 was significantly less in *paf1-1*, *hda6-7*, and *hda6-7 paf1-1* than in Col-0. Notably, the growth of *Psm* ES4326 in *hda6-7 paf1-1* was similar to that of in *paf1-1* and *hda6-7* (Fig. 3C), further supporting the notion that PAF1 and HDA6 function in the same pathway.

Given that both PAF1 and HDA6 bind to *PR1* and they function in the same pathway, we wondered whether the binding of HDA6 at *PR1* depends on PAF1. To this end, we performed eChIP-qPCR analysis using the *35S:HDA6-YFP/paf1-1* transgenic plants, which were obtained by crossing *35S:HDA6-YFP*/Col-0 with *paf1-1*. We found that the abundance of HDA6–yellow fluorescent protein (YFP) at *PR1* in *paf1-1* was significantly lower than that in Col-0 (Fig. 3D), suggesting that PAF1 is required for the recruitment of HDA6 to *PR1*.

Previously, it was reported that HDA6 can effectively remove the acetylation of histone H3 lysine 9 (H3K9ac) in vivo and in vitro (*47*–*50*), and H3K9ac is considered to promote gene expression (*51*, *52*). Therefore, we tested whether H3K9ac is associated with the enhanced defense genes expression in *paf1-1*. To this end, we performed eChIP-seq analysis using the H3K9ac antibody in Col-0 and *paf1-1*. Data analysis revealed that the abundance of H3K9ac at 1045 genes was higher in *paf1-1* than in Col-0 (dataset S7). Among them, 156 genes were up-regulated (fig. S5A and dataset S8) in *paf1-1* compared to Col-0. GO analysis on these 156 genes revealed that the immune-related GO terms (e.g., defense response, response to bacterium, and response to SA) were significantly enriched (fig. S5B

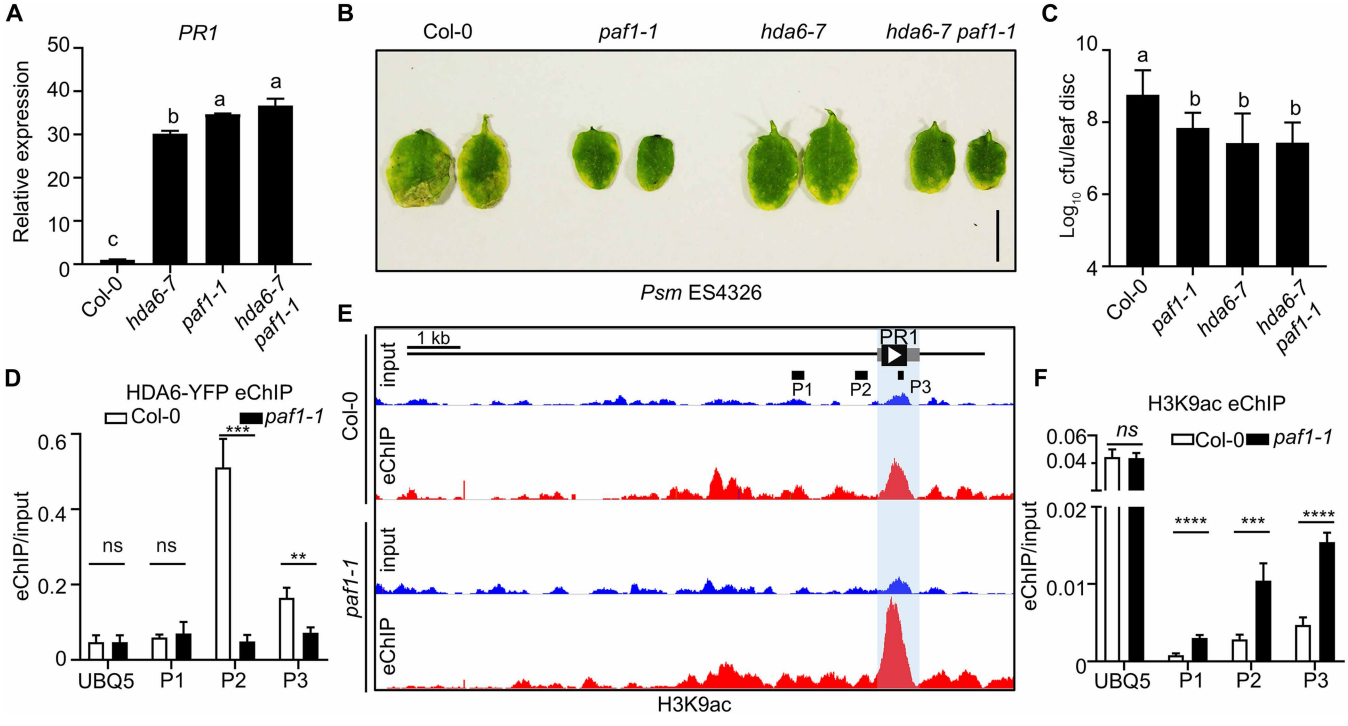

Fig. 3. PAF1 recruits HDA6 to promote H3 deacetylation at defense genes. (**A**) Relative expression of *PR1* in Col-0, *hda6–7*, *paf1–1*, and *hda6-7 paf1-1*. *UBQ5* serves as a reference gene. The data are represented as means ± SD ($n = 3$). Different letters above each bar indicate significant differences determined by one-way ANOVA analysis, followed by Tukey's multiple comparison test ($P < 0.05$). (**B**) Representative leaves at 3 dpi by *Psm* ES4326 ($OD_{600} = 0.001$). Scale bar, 0.5 cm. (**C**) Growth of *Psm* ES4326 in the leaves at 3 dpi. The data are represented as means ± SD ($n = 8$). Different letters above each bar indicate significant differences determined by one-way ANOVA analysis, followed by Tukey's multiple comparison test ($P < 0.05$). (**D** and **F**) eChIP-qPCR assays. The immunoprecipitation was carried out using α-GFP (D) or α-H3K9ac (F) antibody, and the primers used for qPCR are shown in (E). The ratios of eChIP and input are shown. *UBQ5* serves as a negative control. The data are represented as means ± SD ($n = 3$). The statistical significance was determined using a two-tailed Student's t-test. ns, not significant; $^{**}P < 0.01$; $^{***}P < 0.001$; and $^{****}P < 0.0001$. (**E**) eChIP-seq assays. Col-0 and *paf1–1* seedlings were used for eChIP-seq analysis. The immunoprecipitation was carried out using an α-H3K9ac antibody. Both the immunoprecipitated DNA and the input DNA were subjected to next-generation sequencing analysis. P1, P2, and P3 represent the regions used in the eChIP-qPCR assays.

and dataset S9). As expected, the abundance of H3K9ac at *PR1* in *paf1-1* was higher than that in Col-0 (Fig. 3E), which was further confirmed using eChIP-qPCR analysis (Fig. 3F). Collectively, these data demonstrated that PAF1 recruits HDA6 to promote H3 deacetylation at defense genes.

SA promotes the polyubiquitination and degradation of PAF1

Next, we want to know how the repression of PAF1 on *PR1* is derepressed upon pathogen infection. Because SA plays a central role in immune response, we speculated that SA might negatively regulate PAF1. First, we investigated whether SA inhibits the transcription level of *PAF1*. We did SA treatment on the *proPAF1:GUS* transgenic seedlings, in which the *GUS* (β-glucuronidase) gene was driven by the *PAF1* promoter. Based on the GUS staining results (fig. S6A), SA did not affect *PAF1* transcription obviously. This result was further confirmed through RT-qPCR analysis (fig. S6B). Second, we examined whether SA affects the protein level of PAF1. The PAF1-LUC fusion protein was transiently expressed in *Nicotiana benthamiana* leaves. Compared with the mock treatment, the luminescence signals in the leaf half treated with SA markedly decreased (fig. S6C). To further confirm this, we transiently coexpressed mCherry-PAF1 and GFP in *N. benthamiana*. Consistently, we found that after SA treatment, mCherry-PAF1 signals markedly decreased, while the GFP signals did not change obviously (fig. S6D). This result was confirmed in the *35S:PAF1-GFP* transgenic *Arabidopsis* leaves (Fig. 4A). We also validated these results through immunoblotting analysis in *Arabidopsis* protoplasts (fig. S6E) and transgenic lines (Fig. 4B). To exclude the possibility that the decreased PAF1 protein levels after SA treatment were due to the decreased *PAF1* mRNA

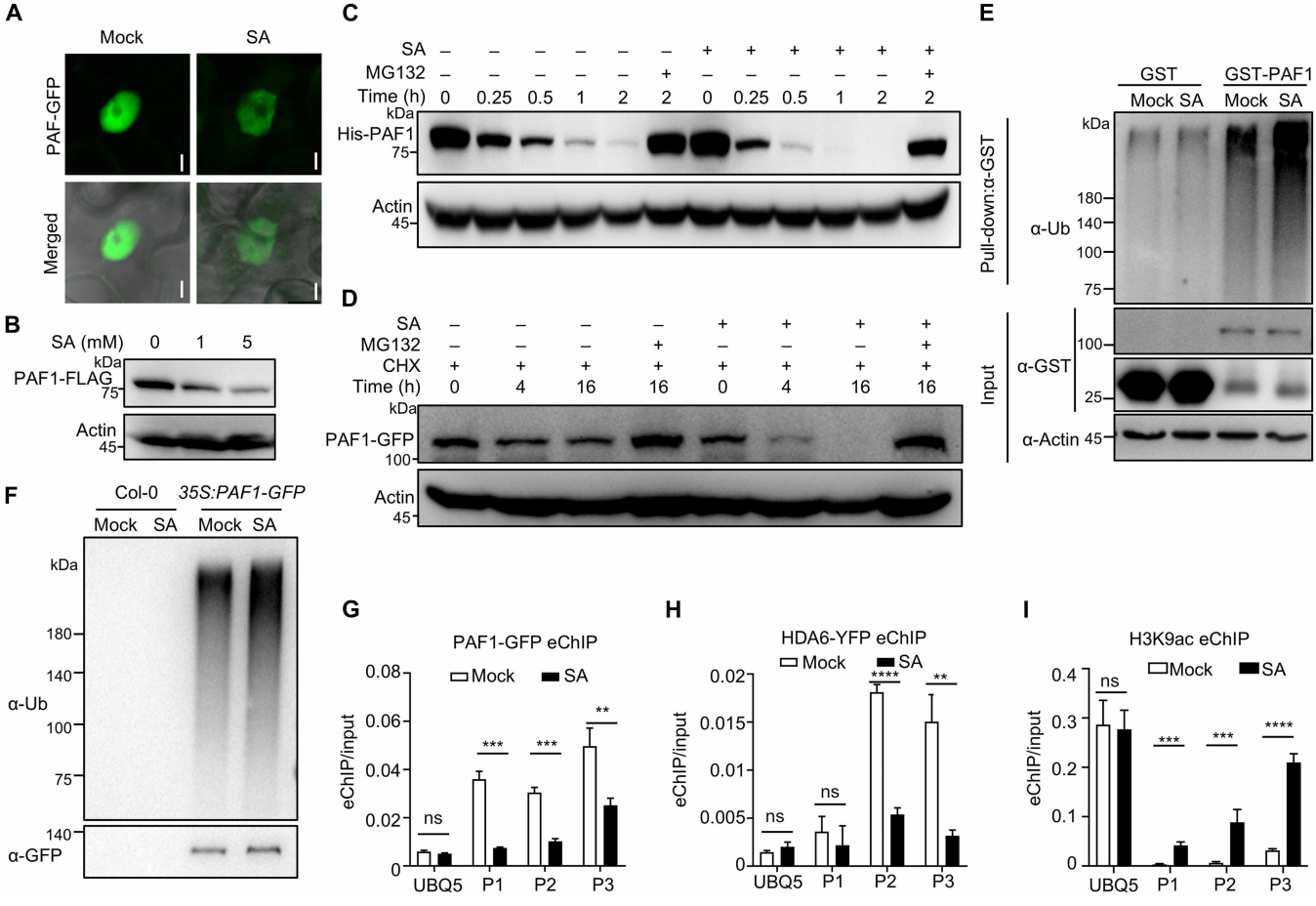

Fig. 4. SA promotes the polyubiquitination and degradation of PAF1. (**A**) Representative images of PAF1-GFP in the *35S:PAF1-GFP*/Col-0 transgenic Arabidopsis treated with or without 1 mM SA for 4 hours. Scale bar, 5 μm. (**B**) Protein level of PAF1-FLAG in the *35S:PAF1-FLAG*/Col-0 transgenic *Arabidopsis* treated with 1 or 5 mM SA for 1 hour. The total proteins were subjected to immunoblotting analysis. (**C**) In vitro protein degradation assays. The recombinant His-PAF1 proteins were incubated with total protein extracts of Col-0 treated with or without 1 mM SA for 4 hours. (**D**) In vivo protein degradation assays. The *35S:PAF1-GFP*/Col-0 transgenic *Arabidopsis* were treated with cycloheximide (CHX; 50 μg/ml), 1 mM SA, or 50 μM MG132. (**E**) Semi–in vitro ubiquitination assays. The recombinant GST and GST-PAF1 proteins coupled with glutathione beads were incubated with the total protein extracts of Col-0 treated with or without 1 mM SA in ubiquitination buffer for 4 hours. After washing, GST and GST-PAF1 proteins were eluted and subjected to immunoblotting analysis using α-Ubiquitin (Ub) antibody. (**F**) In vivo ubiquitination assays. The *35S:PAF1-GFP*/Col-0 transgenic *Arabidopsis* were treated with 50 μM MG132 and/or 1 mM SA for 4 hours. The proteins immunoprecipitated by α-GFP beads were subjected to immunoblotting analysis. (**G** to **I**) eChIP-qPCR assays. The plants were treated with or without 1 mM SA for 4 hours. The immunoprecipitation was carried out using α-GFP [(G) and (H)] or α-H3K9ac (I) antibodies, and the primers used for qPCR are shown in Fig. 1H. The ratios of eChIP and input are shown. *UBQ5* serves as a negative control. The data are represented as means ± SD ($n = 3$). The statistical significance was determined using a two-tailed Student's *t* test. $^{**}P < 0.01$, $^{***}P < 0.001$, and $^{****}P < 0.0001$.

levels, we carried out RT-qPCR analysis, which revealed that SA treatment did not significantly affect the expression of *PAF1* (fig. S7). Together, these results strongly suggested that SA negatively regulates the PAF1 protein level, most likely by promoting its degradation.

To investigate this hypothesis, we conducted protein degradation assays. For the in vitro protein degradation assays, the recombinant His-PAF1 proteins were incubated with *Arabidopsis* extracts in the absence or presence of SA. As shown in Fig. 4C, the degradation of His-PAF1 was faster in the sample with SA, indicating that SA promotes the degradation of PAF1. Notably, the degradation of PAF1 could be blocked by MG132, suggesting that PAF1 is degraded by the proteasome. Next, we monitored PAF1 degradation rate *in planta*. For these assays, the *35S:PAF1-GFP* transgenic *Arabidopsis* seedlings were treated with the translation inhibitor cycloheximide to block protein synthesis. Consistent with the in vitro protein degradation assays, the levels of PAF1-GFP decreased much more markedly in the presence of SA (Fig. 4D). These results indicated SA promotes the degradation of PAF1.

Given that SA promotes PAF1 degradation by the proteasome, we investigated whether SA promotes the polyubiquitination of PAF1. To test this, we first performed semi–in vitro ubiquitination assays. The recombinant glutathione *S*-transferase (GST) and GST-PAF1 proteins coupled with glutathione beads were incubated with *Arabidopsis* extracts in the absence or presence of SA. As shown in Fig. 4E, the polyubiquitination level of GST-PAF1 but not GST was much higher in the sample with SA. To confirm this result in vivo, we transiently expressed GFP and PAF1-GFP in *Arabidopsis* protoplasts in the absence or presence of SA. The GFP and PAF1-GFP proteins immunoprecipitated by α-GFP beads were subjected to immunoblotting analysis. We found that the polyubiquitination level of PAF1-GFP but not GFP was higher in the sample treated with SA (fig. S6F). This result was further confirmed in the experiment using the *35S:PAF1-GFP* transgenic *Arabidopsis* line (Fig. 4F). These results suggested that SA promotes the polyubiquitination of PAF1.

Then, we examined the biological significance of the SA-promoted degradation of PAF1. We performed eChIP-qPCR assays and found that the PAF1 and HDA6 abundance at *PR1* decreased after SA treatment (Fig. 4, G and H), and the H3K9ac abundance at *PR1* increased after SA treatment compared with mock treatment (Fig. 4I).

PAF1 physically interacts with NPR1

Next, we aimed to identify which E3 ubiquitin ligase mediates the polyubiquitination of PAF1. Given that the roles of NPR1 and PAF1 in *PR1* expression are opposite and NPR1 has been shown to function as an E3 ubiquitin ligase (*21*, *27*, *29*), we speculated that NPR1 may mediate the polyubiquitination of PAF1. Thus, we investigated whether PAF1 interacts with NPR1 using different methods, such as Y2H (Fig. 5A), BiFC (Fig. 5B), split luciferase (Fig. 5C), CoIP (Fig. 5D), and protein pull-down assays (Fig. 5E). All these experiments strongly suggested that PAF1 physically interacts with NPR1.

Because NPR1 is an SA receptor, we tested whether SA affects its interaction with PAF1. To this end, we added SA in the interaction assays. For Y2H assays, we used the previously reported SMC5-PAF1 interaction (*42*) as a control. Strikingly, we found that SA promotes the NPR1-PAF1 interaction, but this was not the case for the SMC5-PAF1 interaction (Fig. 5F). We also verified this result through in vitro pull-down (Fig. 5G) and CoIP assays (Fig. 5H). These data indicated that PAF1 interacts with NPR1 and that SA enhances this interaction.

NPR1 promotes the polyubiquitination and degradation of PAF1

To determine whether NPR1 promotes the polyubiquitination of PAF1, we performed ubiquitination assays. In a semi–in vitro ubiquitination assays, GST and GST-PAF1 proteins coupled with the glutathione beads were incubated with protein extracts of either the *npr1-1* mutant or Col-0. We found that the polyubiquitination level of GST-PAF1 but not GST was lower in *npr1-1* than that in Col-0 (Fig. 6A). To further confirm this, we incubated GST and GST-PAF1 with the *npr1-1* extracts adding MBP or MBP-NPR1. Compared to the MBP control, the presence of MBP-NPR1 increased the polyubiquitination level of GST-PAF1 but not GST (Fig. 6B). To investigate whether NPR1 directly mediates the polyubiquitination of PAF1, we conducted in vitro ubiquitination assays using purified GST-PAF1, GST, MBP-CUL3-RBX1, UBA1-His (E1), UBC8-His (E2), His-FLAG-UBQ (Ub), MBP, and/or MBP-NPR1 proteins. We found that the polyubiquitination level of PAF1 increased in the presence of MBP-NPR1 compared with MBP (Fig. 6C), suggesting that NPR1 can directly mediate the polyubiquitination of PAF1.

To test whether NPR1 promotes the polyubiquitination of PAF1 in vivo, we transiently expressed GFP and PAF1-GFP in Col-0 or *npr1-1* protoplasts. GFP and PAF1-GFP were immunoprecipitated by α-GFP beads and subjected to immunoblotting analysis. We found that the polyubiquitination level of PAF1-GFP but not GFP was much lower in *npr1-1* than that in Col-0 (fig. S8A). To further confirm this result, we compared the polyubiquitination levels of PAF1-GFP in the *35S:PAF1-GFP*/Col-0 and *35S:PAF1-GFP/npr1-1* transgenic *Arabidopsis*. As shown in Fig. 6D, the polyubiquitination level of PAF1-GFP in *35S:PAF1-GFP/npr1-1* was much lower than that in *35S:PAF1-GFP*/Col-0.

The NPR1-promoted polyubiquitination of PAF1 indicated that NPR1 may promote PAF1 degradation. To test this, we transiently expressed PAF1-FLAG driven by the 35*S* promoter in Col-0 or *npr1-1* protoplasts. The cyan fluorescent protein (CFP)–hemagglutinin (HA) in the same vector of PAF1-FLAG was used as a control for transfection efficiency. We found the protein level of PAF1-FLAG in *npr1-1* was higher than that in Col-0 (fig. S8B). This difference was not due to the altered mRNA level of *PAF1* in *npr1-1* (fig. S9). To further confirm this result, we obtained the *35S:PAF1-GFP/npr1-1* transgenic plants by crossing *35S:PAF1-GFP*/Col-0 with *npr1-1* and compared the protein levels of PAF1-GFP. As expected, the protein level of PAF1-GFP was higher in *npr1-1* than in Col-0 (Fig. 6E). Furthermore, we carried out in vitro protein degradation assays by incubating the recombinant His-PAF1 proteins with plant extracts of Col-0 or *npr1-1*. As shown in Fig. 6F, the level of His-PAF1 decreased much more markedly in the Col-0 extracts than in the *npr1-1* extracts, suggesting that NPR1 promotes the degradation of PAF1. Altogether, these results provide evidence that NPR1 functions as an E3 ubiquitin ligase to promote the polyubiquitination and degradation of PAF1.

PAF1 functions downstream of NPR1

To further investigate the relationship between NPR1 and PAF1, we compared the transcriptomes regulated by NPR1 or PAF1. We analyzed the previously reported RNA-seq data (*20*) and found that 1026 genes were significantly down-regulated in *npr1-1* compared with Col-0 after SA treatment (dataset S10). These 1026 genes were considered NPR1-activated genes. The 1702 genes up-regulated in

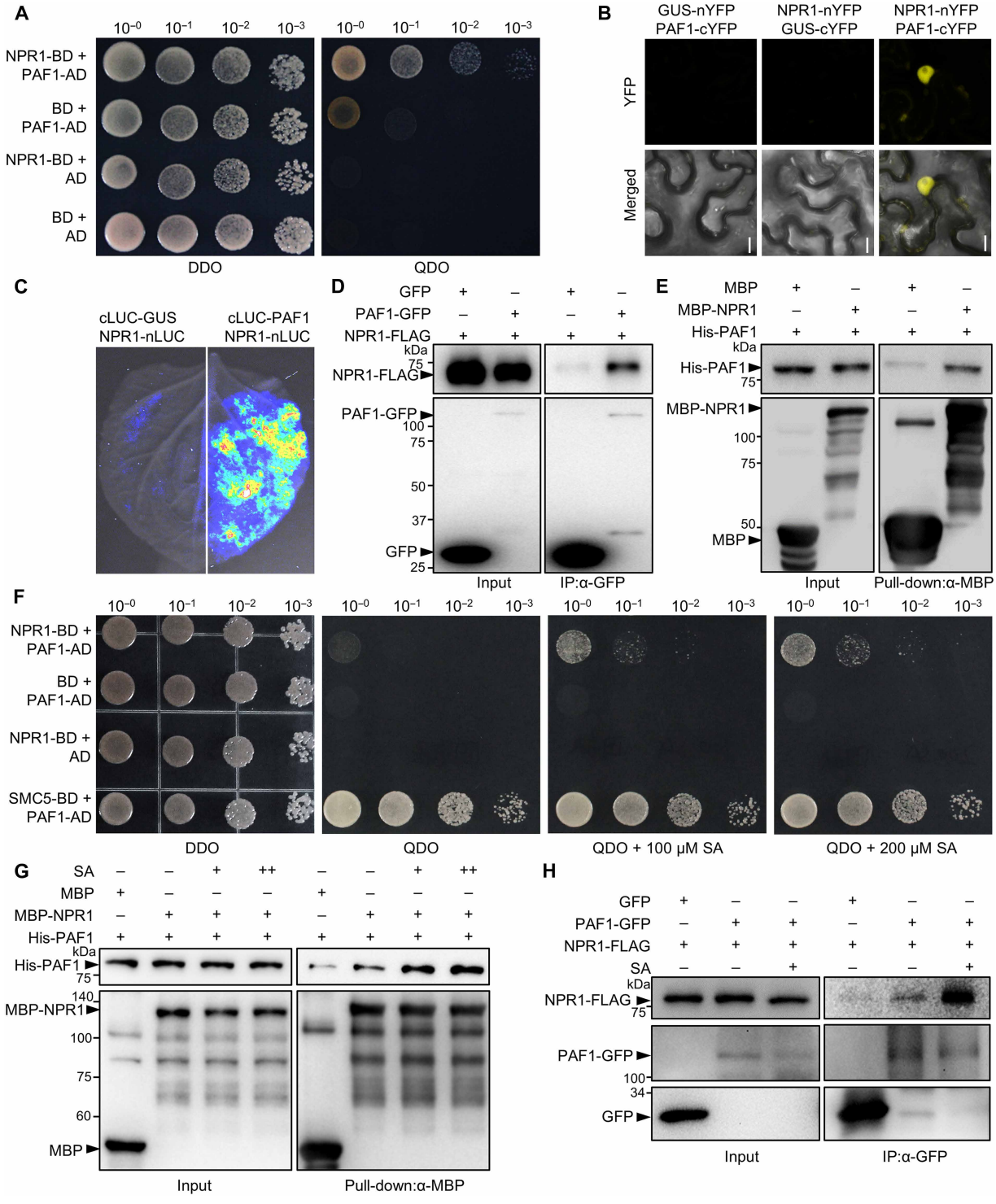

Fig. 5. SA promotes the interaction between PAF1 and NPR1. (**A** and **F**) Y2H assays. The yeasts were grown for 4 days (A) or 3 days (F). (**B**) BiFC assays. The proteins were fused to either the cYFP or nYFP and were transiently expressed in *N. benthamiana*. The YFP fluorescence detected by confocal microscopy indicates interaction. Scale bars, 10 μm. (**C**) Split luciferase assays. The proteins were fused to either the cLUC or nLUC and were transiently expressed in *N. benthamiana*. The luminescence detected by a CCD camera indicates interaction. (**D** and **H**) CoIP assays. NPR1-FLAG was coexpressed with PAF1-GFP or GFP in Col-0 protoplasts. The immunoprecipitation was carried out using α-GFP beads. The protoplasts were treated with or without 1 mM SA for 4 hours (H). (**E** and **G**) Pull-down assays. The MBP-NPR1 or MBP coupled with dextrin beads were incubated with His-PAF1, respectively. 1 mM SA (+) or 5 mM SA (++) was added to the reaction (G).

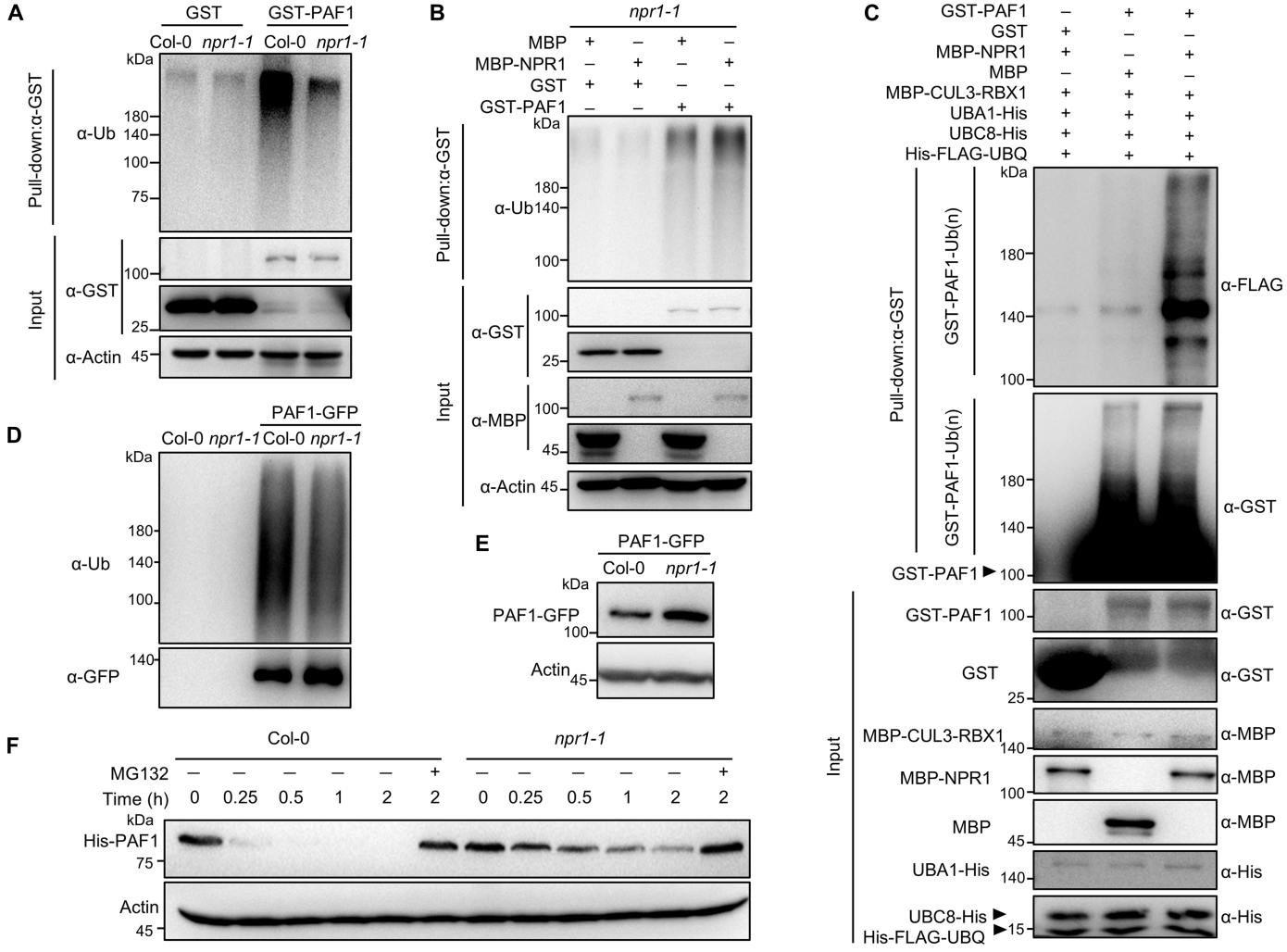

Fig. 6. NPR1 promotes the polyubiquitination and degradation of PAF1. (**A** and **B**) Semi–in vitro ubiquitination assays. The recombinant GST and GST-PAF1 proteins coupled with glutathione beads were incubated with the total protein extracts of Col-0 or *npr1-1* treated with 1 mM SA for 4 hours in ubiquitination buffer for 4 hours. After washing, GST-PAF1 and GST proteins were eluted and subjected to immunoblotting analysis. (**C**) In vitro ubiquitination assays. The recombinant GST and GST-PAF1 proteins coupled with glutathione beads were incubated with the purified MBP-CUL3-RBX1, UBA1-His, UBC8-His, His-FLAG-UBQ, MBP-NPR1, or MBP in the in vitro ubiquitination buffer with 1 mM SA for 2 hours. After washing, GST and GST-PAF1 proteins were eluted and subjected to immunoblotting analysis. (**D**) In vivo ubiquitination assays. The *35S:PAF1-GFP* transgenic plants were treated with 50 μM MG132 and 1 mM SA for 4 hours. The proteins immunoprecipitated by α-GFP beads were subjected to immunoblotting analysis. (**E**) Protein level of PAF1-GFP in *35S:PAF1-GFP*/Col-0 and *35S:PAF1-GFP/npr1-1* transgenic plants treated with 1 mM SA for 4 hours. The total proteins were subjected to immunoblotting analysis. (**F**) In vitro protein degradation assays. The recombinant His-PAF1 proteins were incubated with total protein extracts of Col-0 or *npr1-1* treated with or without 1 mM SA for 4 hours in protein degradation buffer.

the *paf1-1* (dataset S1) were considered PAF1-repressed genes. Venn diagram analysis revealed that 419 genes were activated by NPR1 and repressed by PAF1 (fig. S10A and dataset S11). GO analysis on these 419 genes revealed that the immune-related GO terms (e.g., defense response, response to bacterium, immune system process, and response to SA) were significantly enriched (fig. S10B and dataset S12).

To further validate the above results, we tested the effects of PAF1 and NPR1 on the transcription of *PR1* using dual-luciferase reporter assays. As expected, PAF1-GFP repressed the expression level of *PR1*, whereas NPR1-GFP promoted its expression (Fig. 7, A and B). Compared with NPR1-GFP, the coexpression of both NPR1-GFP and PAF1-GFP significantly reduced the expression level of *PR1*, supporting that PAF1 functions downstream of NPR1. To test this further, we investigated *PR1* expression in the *npr1-1 paf1-1* double mutant plants. Under both mock and SA-treated conditions, the expression level of *PR1* in *npr1-1 paf1-1* was significantly higher than that in *npr1-1* (Fig. 7C).

We have shown that PAF1 bound to *PR1* through eChIP-qPCR assays (Fig. 1H). Since NPR1 promotes PAF1 degradation after SA treatment (Fig. 6), we thus wondered whether the binding of PAF1 to *PR1* is regulated by NPR1. Therefore, we performed eChIP-qPCR assays using the SA-treated *35S:PAF1-GFP/Col-0* and *35S:PAF1-GFP/npr1-1* transgenic plants and found that the PAF1 abundance at *PR1* in *npr1-1* was significantly higher than that in Col-0 (Fig. 7D).

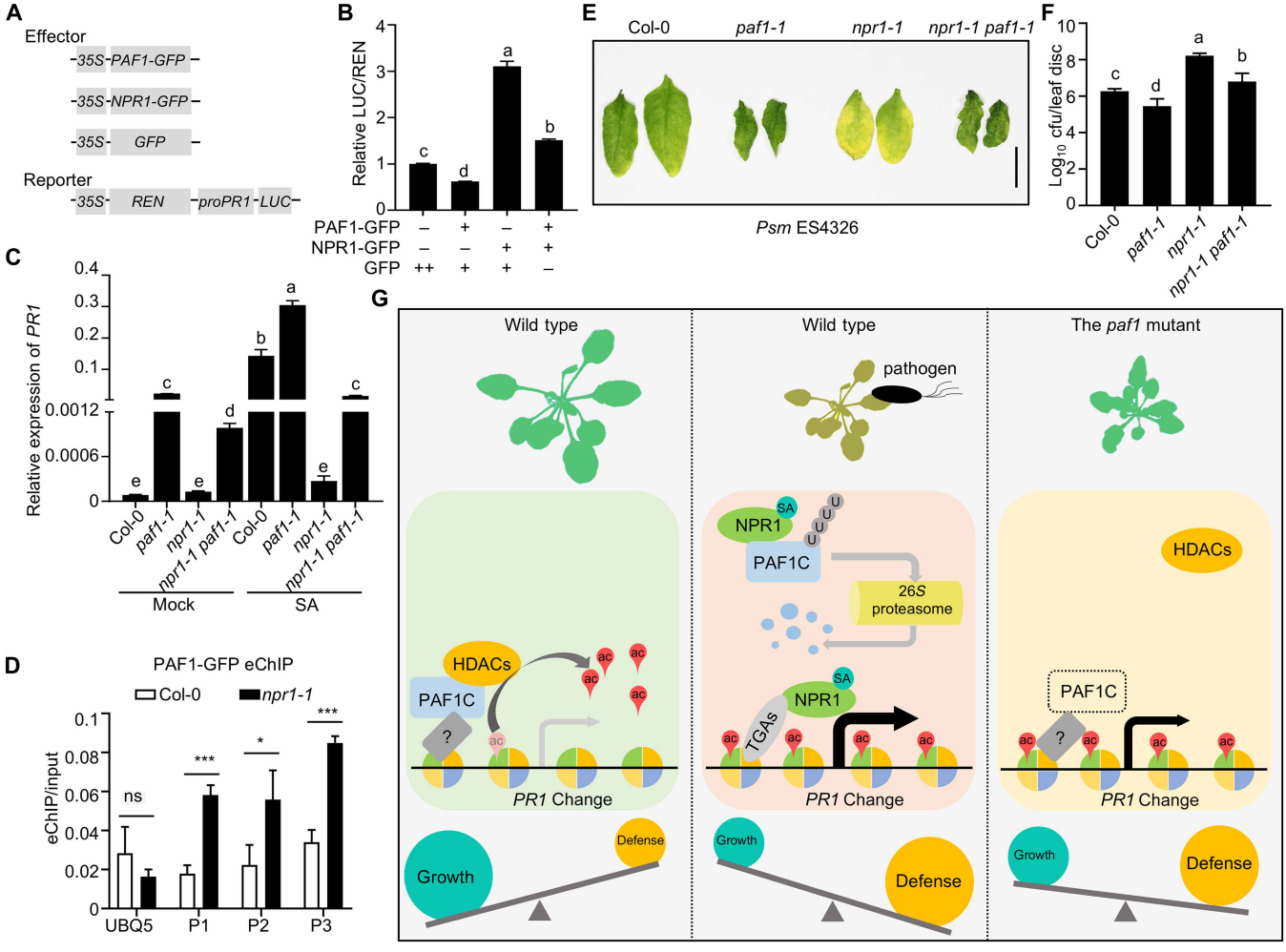

Fig. 7. PAF1 functions downstream of NPR1. (**A**) Schematic representation of the constructs used in the dual-luciferase reporter assays. (**B**) Dual-luciferase reporter assays. The reporter and effectors were coexpressed in *Arabidopsis* protoplasts. The relative LUC activities normalized to the REN activities are shown (LUC/REN). The data are represented as means ± SD ($n = 3$). Different letters above each bar indicate significant differences determined by one-way ANOVA analysis followed by Tukey's multiple comparison test ($P < 0.05$). (**C**) Relative expression of *PR1* in *Arabidopsis* treated with or without 1 mM SA for 4 hours. The data are represented as means SD ($n = 3$). Different letters above each bar indicate significant differences determined by one-way ANOVA analysis followed by Tukey's multiple comparison test ($P < 0.05$). (**D**) eChIP-qPCR assays. *35S:PAF1-GFP*/Col-0 and *35S:PAF1-GFP/npr1-1* were treated with 1 mM SA for 4 hours. The immunoprecipitation was carried out using α-GFP antibody, and the primers used for qPCR are shown in Fig. 1H. The ratios of eChIP and input are shown. *UBQ5* serves as a negative control. The data are represented as means ± SD ($n = 3$). The statistical significance was determined using a two-tailed Student's *t* test. *$P < 0.05$ and ***$P < 0.001$. (**E**) Representative leaves at 3 dpi by *Psm* ES4326 ($OD_{600} = 0.0001$). Scale bar, 0.5 cm. (**F**) Growth of *Psm* ES4326 in the leaves at 3 dpi. The data are represented as means ± SD ($n = 8$). Different letters above each bar indicate significant differences determined by one-way ANOVA analysis followed by Tukey's multiple comparison test ($P < 0.05$). (**G**) Proposed working model.

Last, we examined the disease resistance of *npr1-1 paf1-1* to *Psm* ES4326. Compared with *npr1-1*, the disease symptoms of *npr1-1 paf1-1* was less severe, and the growth of *Psm* ES4326 was significantly reduced (Fig. 7, E and F). Consistently, the plant size and fresh weight of the *npr1-1 paf1-1* were reduced in comparison to *npr1-1* (fig. S11). All these results supported that PAF1 functions downstream of NPR1.

DISCUSSION

We proposed a simplified working model to illustrate how PAF1 balances plant defense and growth (Fig. 7G). Under normal growth conditions, PAF1 interacts with and recruits HDACs to defense genes such as *PR1*, where HDACs promote histone deacetylation, thereby repressing the expression of defense genes to inhibit defense and promote growth. When plants are attacked by pathogens, the increased SA level promotes the interaction between PAF1 and NPR1, which mediates the polyubiquitination and degradation of PAF1 to derepress defense genes, thereby promoting defense and inhibit growth.

Plants regulate growth-defense tradeoff through multiple mechanisms. One of the key aspects is to repress defense genes expression in the absence of pathogen infections, and this repression needs to be rapidly removed upon pathogen infection. We showed here PAF1 can repress defense genes expression and is degraded after SA treatment. In this view, PAF1 is an ideal regulator of the growth-defense tradeoff, which can potentially offer important agronomical perspectives.

PAF1C is highly conserved in eukaryotes (*36*). However, the function of PAF1C is still not well-studied, especially in plants. In *Arabidopsis*, the best-characterized function of PAF1C is to repress flowering by promoting the expression of *FLC* (*33*). We recently found that PAF1C is also involved in DNA damage repair (*42*). In the current study, we found that PAF1C is a negative regulator of plant immunity. Given the conservation of PAF1C in plants, this function of PAF1C may apply to other plant species.

It is well-known that PAF1 can promote gene transcription by mediating H2B mono-ubiquitination (*37*, *43*, *53*–*56*). In sharp contrast, here we found that PAF1 can also repress gene transcription by mediating H3K9 deacetylation (Fig. 3). In addition to H3K9ac, there are other forms of histone acetylation such as H3K4ac, H3K14ac, H3K27ac, and H3K36ac (*47*). We found that PAF1 interacted with several HDACs (fig. S4). These HDACs may function with PAF1 to regulate different forms of histone acetylation and participate in different biological processes. It remains to be determined whether the repression activity of PAF1C is conserved in other eukaryotes. Nevertheless, our study challenges the current view on the molecular function of PAFC1 in gene expression.

As an SA receptor, NPR1 is the master regulator of plant immune responses (*21*). NPR1 can function as a transcriptional co-activator to promote the expression of defense genes by interacting with transcription factors. NPR1 can also function as an E3 ubiquitin ligase to mediate protein polyubiquitination and degradation. Compared with transcription regulation, the role of NPR1 as an E3 ubiquitin ligase is less understood. So far, only a few proteins have been identified as substrates of NPR1, including EDS1, NIMIN1, WRKY54, WRKY70, and GID1 (*27*, *29*). Here, we revealed that PAF1 was another substrate of NPR1. Notably, the loss of PAF1 did not fully suppress *npr1-1* (Fig. 7), suggesting that NPR1 functions by mediating the polyubiquitination and degradation of other proteins that still need to be identified.

MATERIALS AND METHODS

Plant materials and growth conditions

All *Arabidopsis* mutants used in this study are in the *Columbia-0* (Col-0) background. The *vip3-2* (SALK_139885) and *cdc73-1* (SALK_150644) were obtained from Arashare (www.arashare.cn/). The *paf1-1* (*ddrm4-1*), *npr1-1*, *vip5-2* (SALK_062223), *vip4-c1*, *vip6-c1*, and *hda6-7* mutants were described previously (*29*, *42*, *57*). All the transgenic plants were generated using the floral-dip method (*58*). Seeds were sterilized with 2% plant preservative mixture (Plant Cell Technology), stratified at 4°C in the dark for 2 days, and then plated on half-strength (one-half) Murashige and Skoog (MS) medium containing 1% sucrose and 0.35% phytagel (#CP8581Z, Coolaber). Plants were grown under long-day conditions (16 hour of light and 8 hour of dark) in a growth chamber at 22°C.

Pathogen infection

Pathogen infection was carried out as previously described (*59*). Briefly, *P. syringae* pv. *maculicola* ES4326 (*Psm* ES4326) was infiltrated into 3- to 4-week-old leaves using a needle-less syringe. The number of *Psm* ES4326 was determined 3 days after infection.

RNA extraction, RT-qPCR, and RNA-seq

The total RNA was isolated using the RNA Purification Kit (#RN2802, Aidlab Biotech). The cDNA was synthesized using the First-Strand cDNA Synthesis Kit (#DLR101, Beijing Tsingke Biotech). The qPCR was performed using ArtiCan^{CEO}SYBR qPCR Mix (#DLQ101, Beijing Tsingke Biotech) and detected by Fluorescent Quantitative PCR Detection System (#Q2000B, LongGene). *UBQ5* was used as the reference gene. Relative expression levels were calculated using the $2^{-\Delta\Delta CT}$ method. For RNA-seq, 10-day-old seedlings of Col-0 and *paf1-1* grown vertically on one-half MS medium were used. The sequencing library was constructed using the DNA Library Prep Kit for Illumina (#ND627, Vazyme). The sequencing was completed by JMDNA (Shanghai) Bio-Medical Technology using the HiSeq4000 system. Raw reads were processed and aligned to the Arabidopsis reference genome TAIR 10 (www.arabidopsis.org) using STAR (version 2.7.11b). Genes with over 20 reads were filtered and processed using DESeq2 to identify the differentially expressed genes ($P < 0.05$, $|\mathrm{Log_2FoldChange}| > 1$). GO analysis was carried out using PANTHER Classification System database (http://pantherdb.org/).

Vector construction

All constructs were generated using the Lighting Cloning Kit (#BDIT0014, Biodragon Immunotechnology). The primers used for cloning are listed in dataset S13. For Y2H assays, the coding sequences (CDSs) of *HDT1/2/3/4*, *HDA6/7/9/19*, and *NPR1* were cloned into the *pGBKT7* vector digested with Eco RI/Bam HI, and the CDS of *PAF1* was cloned into the *pGADT7* vector digested with Eco RI/Bam HI. For BiFC assays, the CDS of *HDA6* and *NPR1* were cloned into the *pSPYNE-35S* vector digested with Bam HI/Sal I. For split luciferase assays, the CDS of *HDA6* and *NPR1* were cloned into the *pJW771* vector digested with Kpn I and Sal I. For CoIP assays, the CDS of *HDA6* and *YFP* were cloned into the *pFGC5941* vector digested with Nco I and Xba I, and the CDS of *NPR1* was cloned into the *pCambia2306-FLAG* vector digested with Bam HI/Sal I. For protein expression in *Escherichia coli*, the CDS of *HDA6* was cloned into the *pMAL-C2X* vector digested with Eco RI and Sal I. For in vitro ubiquitination assays, the CDS of *PAF1* was cloned into the *pGEX-6P-1* vector digested with Bam HI/Not I. For β-glucuronidase (GUS) staining, the 2-kb promoter of *PAF1* was cloned into the *pCambia2300-GUS* vector digested with Bam HI/Kpn I. For protein expression assays, the CDS of *PAF1* fused with *FLAG* was cloned into the *pFGC5941-CFP-HA* vector digested with Nco I/Pac I. For dual-luciferase reporter assays, the 2-kb promoter of *PR1* was cloned into the *pGreenII-0800-LUC* vector digested with Kpn I/Sal I.

Transient expression

Transient expression in *Arabidopsis* protoplasts was performed as described previously (*60*). For transient expression in *N. benthamiana*, the *Agrobacterium tumefaciens GV3101* containing the indicated vectors was resuspended in infiltration buffer [10 mM MES (pH 5.7), 10 mM $MgCl_2$, and 0.1 mM acetosyringone], incubated at 28°C for 2 hours, and infiltrated into 3- to 4-week-old leaves using a needle-less syringe. The leaves were sampled for subsequent experiments 2 days after infiltration.

Dual-luciferase reporter assays

The dual-luciferase reporter assays was carried out as described previously (*61*). The assays was performed using the Dual Luciferase Reporter Assay Kit (#E1980, Promega). The luciferase activities were measured using a multimode microplate reader (Mithras LB940, Berthold Technologies). The relative LUC activities normalized to the REN activities were calculated.

eChIP-qPCR and eChIP sequencing

The eChIP assays were performed as previously described with some modifications (*62*). Chromatin was sonicated using the Bioruptor Plus sonication system (Diagenode, Belgium). The immunoprecipitation was performed using the protein G beads (#C600022-0001, BBI) coupled with an α-GFP antibody (#11814460001, Roche) or an α-H3K9ac antibody (#ab10812, Abcam). The purified DNA samples were subjected to qPCR analysis or next-generation sequencing. The sequencing library was constructed using the DNA Library Prep Kit for Illumina (#ND627, Vazyme). The sequencing was completed by JMDNA (Shanghai) Bio-Medical Technology using the HiSeq4000 system. The sequencing data were analyzed as follows: The low-quality reads were excluded after quality control by fastqc, and adapters were removed by fastp; high-quality reads were mapped to the Arabidopsis reference genome TAIR 10 (www.arabidopsis.org) using Burrows-Wheeler Aligner (version 0.7.17); duplicate reads were removed by Sambamba; MACS2 was used to detect peaks; HOMER was used to annotate Peaks. The eChIP-seq data were normalized on the basis of reads per kilobase per million mapped reads.

Protein interaction analysis

The Y2H assays, BiFC assays, split luciferase assays, CoIP assays, and pull-down assays were performed as described previously (*59*, *63*, *64*). For Y2H assays, the corresponding constructs were cotransformed into the yeast strain AH109. For CoIP assays, the fusion proteins were transiently expressed in *N. benthamiana* or *Arabidopsis* protoplasts. The α-GFP beads (#L-1016, Biolinkedin) were used for immunoprecipitation. For pull-down assays, all recombinant proteins were expressed in *E. coli* BL21 (DE3). The MBP-tagged proteins coupled to Dextrin beads (#SA026005, Smart-Lifesciences) were used to pull down His-tagged proteins. For BiFC assays, the fusion proteins were coexpressed in *N. benthamiana*. The YFP fluorescence was examined using confocal laser scanning microscopy (TCS SP8, Leica). For split luciferase assays, the fusion proteins were coexpressed in *N. benthamiana*. The luminescences were captured using the Lumazone Imaging System equipped with a 2048B charge-coupled device camera (Roper).

In vivo protein degradation assay

The *35S:PAF1-GFP*/Col-0 transgenic *Arabidopsis* were treated with cycloheximide (50 μg/ml; #T1225, TargetMol, USA), 1 mM SA, and/or 50 μM MG132 (#133407-82-6, Aladdin) for 0, 4, or 16 hours. The total proteins were subjected to immunoblotting using α-GFP and α-actin (#AC009, ABclonal) antibodies.

In vitro protein degradation assays

The recombinant His-PAF1 proteins were incubated with the total protein extracts in protein degradation buffer [25 mM tris-HCl (pH 7.5), 10 mM NaCl, 10 mM $MgCl_2$, 1 mM phenylmethylsulfonyl fluoride (PMSF), 1 mM dithiothreitol (DTT), 2 mM adenosine 5′-triphosphate (ATP)] at 22°C for the indicated time. The total protein extracts were sampled from 8-day-old Col-0 or *npr1-1* treated with or without 1 mM SA for 4 hours. The samples were subjected to immunoblotting analysis using α-His (#2366, Cell Signaling Technology) or α-actin antibodies.

In vivo ubiquitination assays

The plant samples were treated with 50 μM MG132 and/or 1 mM SA for 4 hours. The total proteins extracted with radioimmunoprecipitation assay lysis buffer [50 mM tris-HCl (pH 7.5), 150 mM NaCl, 1% Triton X-100, 1% sodium deoxycholate, 0.1% SDS, 1× protease inhibitor, 2 mM PMSF, 2 mM DTT, and 50 μM MG132] were incubated with α-GFP beads at 4°C for 2 hours. The beads were washed three times with washing buffer [50 mM tris-HCl (pH 7.4), 1 M NaCl, 1% Triton X-100, 1% sodium deoxycholate, 0.1% SDS, and 50 μM MG132] and boiled in 1× SDS loading buffer, followed by immunoblotting analysis using α-ubiquitin (#3936, Cell Signaling Technology) or α-GFP (#11814460001, Roche) antibodies.

Semi–in vitro ubiquitination assays

The GST and GST-PAF1 proteins coupled with glutathione beads (#SA008005, Smart-Lifesciences) were incubated with total protein extracts in ubiquitination buffer [25 mM tris-HCl (pH 7.5), 10 mM NaCl, 10 mM $MgCl_2$, 2 mM PMSF, 2 mM DTT, 4 mM ATP, 50 μM MG132, and 1× protease inhibitor cocktail] at 22°C for 4 hours. The total protein extracts were sampled from 8-day-old Col-0 or *npr1-1* treated with or without 1 mM SA for 4 hours. MBP-NPR1 or MBP was added to the ubiquitination buffer. The beads were washed three times with washing buffer [50 mM tris-HCl (pH 7.4), 1 M NaCl, 1% Triton X-100, 1% sodium deoxycholate, 0.1% SDS, and 50 μM MG132] and boiled in 1× SDS loading buffer, followed by immunoblotting using an α-ubiquitin antibody. The input samples were subjected to immunoblotting using α-actin, α-GST (#AE001, ABclonal), or α-MBP (#AE016, ABclonal) antibodies.

In vitro ubiquitination assays

In vitro ubiquitination assays was carried out as described previously (*29*). The recombinant UBA1-His (E1), UBC8-His (E2), and His-FLAG-UBQ (Ub) proteins were purified using Ni-agarose beads (#SA052005, Smart-Lifesciences). MBP-NPR1, MBP, and MBP-CUL3-RBX1 were purified using dextrin beads (#SA026005, Smart-Lifesciences). The GST and GST-PAF1 proteins coupled with glutathione beads were incubated with the purified UBA1-His, UBC8-His, His-FLAG-UBQ, MBP-CUL3-RBX1, and MBP-NPR1 or MBP in the in vitro ubiquitination buffer [80 mM tris-HCl (pH 7.5), 12 mM ATP, and 1 mM SA] at 24°C for 2 hours. The beads were washed three times with washing buffer [50 mM tris-HCl (pH 7.4), 1 M NaCl, 1% Triton X-100, 1% sodium deoxycholate, and 0.1% SDS] and boiled in 1× SDS loading buffer, followed by immunoblotting using α-GST or α-FLAG (#AE126, ABclonal) antibodies. The input samples were subjected to immunoblotting using α-His, α-GST, or α-MBP antibodies.

Statistical analysis

The statistical analysis was performed using GraphPad Prism version 8 (GraphPad Software; www.graphpad.com). Significance analysis was performed with two-tailed Student's *t* test or one-way analysis of variance (ANOVA), followed by Tukey's multiple comparison tests.

Supplementary Materials

The PDF file includes:

Figs. S1 to S11

Legends for datasets S1 to S13

Other Supplementary Material for this manuscript includes the following:

Datasets S1 to S13

REFERENCES AND NOTES

1. Y. Ding, D. Shaholli, Z. Mou, A large-scale genetic screen for mutants with altered salicylic acid accumulation in Arabidopsis. *Front. Plant Sci.* **5**, 763 (2015).
2. C. Zipfel, Early molecular events in PAMP-triggered immunity. *Curr. Opin. Plant Biol.* **12**, 414–420 (2009).
3. J. D. G. Jones, J. L. Dangl, The plant immune system. *Nature* **444**, 323–329 (2006).
4. W. E. Durrant, X. Dong, Systemic acquired resistance. *Annu. Rev. Phytopathol.* **42**, 185–209 (2004).
5. B. Huot, J. Yao, B. L. Montgomery, S. Y. He, Growth-defense tradeoffs in plants: A balancing act to optimize fitness. *Mol. Plant* **7**, 1267–1287 (2014).
6. J. Chakraborty, P. Ghosh, S. Das, Autoimmunity in plants. *Planta* **248**, 751–767 (2018).
7. S. Hou, T. Thiergart, N. Vannier, F. Mesny, J. Ziegler, B. Pickel, S. Hacquard, A microbiota-root-shoot circuit favours Arabidopsis growth over defence under suboptimal light. *Nat Plants* **7**, 1078–1092 (2021).
8. M. Gao, Y. He, X. Yin, X. Zhong, B. Yan, Y. Wu, J. Chen, X. Li, K. Zhai, Y. Huang, X. Gong, H. Chang, S. Xie, J. Liu, J. Yue, J. Xu, G. Zhang, Y. Deng, E. Wang, D. Tharreau, G. L. Wang, W. Yang, Z. He, Ca^{2+} sensor-mediated ROS scavenging suppresses rice immunity and is exploited by a fungal effector. *Cell* **184**, 5391–5404.e17 (2021).
9. A. Best, A. White, M. Boots, Maintenance of host variation in tolerance to pathogens and parasites. *Proc. Natl. Acad. Sci. U.S.A.* **105**, 20786–20791 (2008).
10. Z. Tang, S. Shi, R. Niu, Y. Zhou, Z. Wang, R. Fu, R. Mou, S. Chen, P. Ding, G. Xu, Alleviating protein-condensation-associated damage at the endoplasmic reticulum enhances plant disease tolerance. *Cell Host Microbe* **32**, 1552–1565.e8 (2024).
11. I. Pagan, F. Garcia-Arenal, Tolerance of plants to pathogens: A unifying view. *Annu. Rev. Phytopathol.* **58**, 77–96 (2020).
12. Z. Tang, R. Mou, G. Xu, Defense strategies for plant health: Disease resistance and tolerance. *Plant Cell* **37**, koaf186 (2025).
13. A. C. Vlot, D. M. A. Dempsey, D. F. Klessig, Salicylic acid, a multifaceted hormone to combat disease. *Annu. Rev. Phytopathol.* **47**, 177–206 (2009).
14. J. Catinot, A. Buchala, E. Abou-Mansour, J.-P. Métraux, Salicylic acid production in response to biotic and abiotic stress depends on isochorismate in Nicotiana benthamiana. *FEBS Lett.* **582**, 473–478 (2008).
15. M. A. Strawn, S. K. Marr, K. Inoue, N. Inada, C. Zubieta, M. C. Wildermuth, Arabidopsis isochorismate synthase functional in pathogen-induced salicylate biosynthesis exhibits properties consistent with a role in diverse stress responses. *J. Biol. Chem.* **282**, 5919–5933 (2007).
16. M. C. Wildermuth, J. Dewdney, G. Wu, F. M. Ausubel, Isochorismate synthase is required to synthesize salicylic acid for plant defence. *Nature* **414**, 562–565 (2001).
17. X. Dong, NPR1, all things considered. *Curr. Opin. Plant Biol.* **7**, 547–552 (2004).
18. C. M. J. Pieterse, L. C. Van Loon, NPR1: The spider in the web of induced resistance signaling pathways. *Curr. Opin. Plant Biol.* **7**, 456–464 (2004).
19. Z. Q. Fu, S. Yan, A. Saleh, W. Wang, J. Ruble, N. Oka, R. Mohan, S. H. Spoel, Y. Tada, N. Zheng, X. Dong, NPR3 and NPR4 are receptors for the immune signal salicylic acid in plants. *Nature* **486**, 228–232 (2012).
20. Y. Ding, T. Sun, K. Ao, Y. Peng, Y. Zhang, X. Li, Y. Zhang, Opposite roles of salicylic acid receptors NPR1 and NPR3/NPR4 in transcriptional regulation of plant immunity. *Cell* **173**, 1454–1467.e15 (2018).
21. S. H. Spoel, X. Dong, Salicylic acid in plant immunity and beyond. *Plant Cell* **36**, 1451–1464 (2024).
22. C. Johnson, E. Boden, J. Arias, Salicylic acid and NPR1 induce the recruitment of trans-activating TGA factors to a defense gene promoter in Arabidopsis. *Plant Cell* **15**, 1846–1858 (2003).
23. S. Kumar, R. Zavaliev, Q. Wu, Y. Zhou, J. Cheng, L. Dillard, J. Powers, J. Withers, J. Zhao, Z. Guan, M. J. Borgnia, A. Bartesaghi, X. Dong, P. Zhou, Structural basis of NPR1 in activating plant immunity. *Nature* **605**, 561–566 (2022).
24. Y. Liu, T. Sun, Y. Sun, Y. Zhang, A. Radojičić, Y. Ding, H. Tian, X. Huang, J. Lan, S. Chen, A. R. Orduna, K. Zhang, R. Jetter, X. Li, Y. Zhang, Diverse roles of the salicylic acid receptors NPR1 and NPR3/NPR4 in plant immunity. *Plant Cell* **32**, 4002–4016 (2020).
25. R. Geyer, S. Wee, S. Anderson, J. Yates, D. A. Wolf, BTB/POZ domain proteins are putative substrate adaptors for cullin 3 ubiquitin ligases. *Mol. Cell* **12**, 783–790 (2003).
26. L. Pintard, A. Willems, M. Peter, Cullin-based ubiquitin ligases: Cul3–BTB complexes join the family. *EMBO J.* **23**, 1681–1687 (2004).
27. R. Zavaliev, R. Mohan, T. Chen, X. Dong, Formation of NPR1 condensates promotes cell survival during the plant immune response. *Cell* **182**, 1093–1108.e18 (2020).
28. P. Genschik, I. Sumara, E. Lechner, The emerging family of CULLIN3-RING ubiquitin ligases (CRL3s): Cellular functions and disease implications. *EMBO J.* **32**, 2307–2320 (2013).
29. X. Yu, X. Cui, C. Wu, S. Shi, S. Yan, Salicylic acid inhibits gibberellin signaling through receptor interactions. *Mol. Plant* **15**, 1759–1771 (2022).
30. Y. Cao, L. Ma, Conservation and divergence of the histone H2B monoubiquitination pathway from yeast to humans and plants. *Front. Biol.* **6**, 109–117 (2011).
31. F. Chen, B. Liu, L. Guo, X. Ge, W. Feng, D.-F. Li, H. Zhou, J. Long, Biochemical insights into Paf1 complex–induced stimulation of Rad6/Bre1-mediated H2B monoubiquitination. *Proc. Natl. Acad. Sci. U.S.A.* **118**, e2025291118 (2021).
32. Y. He, M. R. Doyle, R. M. Amasino, PAF1-complex-mediated histone methylation of Flowering Locus C chromatin is required for the vernalization-responsive, winter-annual habit in *Arabidopsis*. *Genes Dev.* **18**, 2774–2784 (2004).
33. S. Oh, H. Zhang, P. Ludwig, S. van Nocker, A mechanism related to the yeast transcriptional regulator Paf1c is required for expression of the Arabidopsis FLC/MAFMADS box gene family. *Plant Cell* **16**, 2940–2953 (2004).
34. X. Yu, S. D. Michaels, The *Arabidopsis* Paf1c complex component CDC73 participates in the modification of flowering locus C Chromatin. *Plant Physiol.* **153**, 1074–1084 (2010).
35. H. Zhang, S. Van Nocker, The vernalization independence 4 gene encodes a novel regulator of Flowering locus C. *Plant J.* **31**, 663–673 (2002).
36. S. Obermeyer, H. Kapoor, H. Markusch, K. D. Grasser, Transcript elongation by RNA polymerase II in plants: Factors, regulation and impact on gene expression. *Plant J.* **118**, 645–656 (2024).
37. J. A. Jaehning, The Paf1 complex: Platform or player in RNA polymerase II transcription? *Biochim. Biophys. Acta* **1799**, 379–388 (2010).
38. A. M. Francette, S. A. Tripplehorn, K. M. Arndt, The Paf1 complex: A keystone of nuclear regulation operating at the interface of transcription and chromatin. *J. Mol. Biol.* **433**, 166979 (2021).
39. Y. Cao, Y. Dai, S. Cui, L. Ma, Histone H2B monoubiquitination in the chromatin of flowering locus regulates flowering time in *Arabidopsis*. *Plant Cell* **20**, 2586–2602 (2008).
40. Y. Li, J. Yang, X. Shang, W. Lv, C. Xia, C. Wang, J. Feng, Y. Cao, H. He, L. Li, L. Ma, SKIP regulates environmental fitness and floral transition by forming two distinct complexes in Arabidopsis. *New Phytol.* **224**, 321–335 (2019).
41. C. Lu, Y. Tian, S. Wang, Y. Su, T. Mao, T. Huang, Q. Chen, Z. Xu, Y. Ding, Phosphorylation of SPT5 by CDKD;2 is required for VIP5 recruitment and normal flowering in *Arabidopsis thaliana*. *Plant Cell* **29**, 277–291 (2017).
42. C. Li, Y. Guo, L. Wang, S. Yan, The SMC5/6 complex recruits the PAF1 complex to facilitate DNA double-strand break repair in *Arabidopsis*. *EMBO J.* **42**, e112756 (2023).
43. W. Antosz, A. Pfab, H. F. Ehrnsberger, P. Holzinger, K. Köllen, S. A. Mortensen, A. Bruckmann, T. Schubert, G. Längst, J. Griesenbeck, V. Schubert, M. Grasser, K. D. Grasser, The composition of the *Arabidopsis* RNA polymerase II transcript elongation complex reveals the interplay between elongation and mRNA processing factors. *Plant Cell* **29**, 854–870 (2017).
44. Z. Wang, H. Cao, F. Chen, Y. Liu, The roles of histone acetylation in seed performance and plant development. *Plant Physiol. Biochem.* **84**, 125–133 (2014).
45. X. Cui, A. Dard, J. P. Reichheld, D. X. Zhou, Multifaceted functions of histone deacetylases in stress response. *Trends Plant Sci.* **28**, 1245–1256 (2023).
46. R. Pandey, Analysis of histone acetyltransferase and histone deacetylase families of Arabidopsis thaliana suggests functional diversification of chromatin modification among multicellular eukaryotes. *Nucleic Acids Res.* **30**, 5036–5055 (2002).
47. V. Kumar, J. K. Thakur, M. Prasad, Histone acetylation dynamics regulating plant development and stress responses. *Cell. Mol. Life Sci.* **78**, 4467–4486 (2021).
48. Y. Wang, Q. Hu, Z. Wu, H. Wang, S. Han, Y. Jin, J. Zhou, Z. Zhang, J. Jiang, Y. Shen, H. Shi, W. Yang, HISTONE DEACETYLASE 6 represses pathogen defence responses in *Arabidopsis thaliana*. *Plant Cell Environ.* **40**, 2972–2986 (2017).
49. W. Li, X. Zhang, Q. Zhang, Q. Li, Y. Li, Y. Lv, Y. Liu, Y. Cao, H. Wang, X. Chen, H. Yang, Pickle and histone deacetylase 6 coordinately regulate genes and transposable elements in Arabidopsis. *Plant Physiol.* **196**, 1080–1094 (2024).
50. Q. Wang, X. Bao, S. Chen, H. Zhong, Y. Liu, L. Zhang, Y. Xia, F. Kragler, M. Luo, X. D. Li, H. M. Lam, S. Zhang, AtHDA6 functions as an H3K18ac eraser to maintain pericentromeric CHG methylation in *Arabidopsis thaliana*. *Nucleic Acids Res.* **49**, 9755–9767 (2021).
51. J. Zhou, X. Wang, K. He, J. B. Charron, A. A. Elling, X. W. Deng, Genome-wide profiling of histone H3 lysine 9 acetylation and dimethylation in Arabidopsis reveals correlation between multiple histone marks and gene expression. *Plant Mol. Biol.* **72**, 585–595 (2010).
52. M. Benhamed, C. Bertrand, C. Servet, D. X. Zhou, Arabidopsis GCN5, HD1, and TAF1/HAF2 interact to regulate histone acetylation required for light-responsive gene expression. *Plant Cell* **18**, 2893–2903 (2006).
53. S. M. Vos, L. Farnung, M. Boehning, C. Wigge, A. Linden, H. Urlaub, P. Cramer, Structure of activated transcription complex Pol II–DSIF–PAF–SPT6. *Nature* **560**, 607–612 (2018).
54. Z. Nasim, H. Susila, S. Jin, G. Youn, J. H. Ahn, Polymerase II–associated factor 1 complex-regulated Flowering Locus C-clade genes repress flowering in response to chilling. *Front. Plant Sci.* **13**, 817356 (2022).
55. G. Fuchs, M. Oren, Writing and reading H2B monoubiquitylation. *Biochim. Biophys. Acta* **1839**, 694–701 (2014).
56. N. Blanco-Tourinan, J. Perez-Alemany, C. Bourbousse, D. Latrasse, O. Ait-Mohamed, M. Benhamed, F. Barneche, M. A. Blazquez, J. Gallego-Bartolome, D. Alabadi, The plant ploymerase-associated factor 1complex links transcription and H2B monoubiquitination genome wide. *Plant Physiol.* **195**, 640–651 (2024).

57. T. Hu, D. Manuela, V. Hinsch, M. Xu, PICKLE associates with histone deacetylase 9 to mediate vegetative phase change in Arabidopsis. *New Phytol.* **235**, 1070–1081 (2022).
58. S. J. Clough, A. F. Bent, Floral dip: A simplified method for *Agrobacterium*-mediated transformation of *Arabidopsis thaliana*. *Plant J.* **16**, 735–743 (1998).
59. S. Yan, W. Wang, J. Marqués, R. Mohan, A. Saleh, W. E. Durrant, J. Song, X. Dong, Salicylic acid activates DNA damage responses to potentiate plant immunity. *Mol. Cell* **52**, 602–610 (2013).
60. S. D. Yoo, Y. H. Cho, J. Sheen, Arabidopsis mesophyll protoplasts: A versatile cell system for transient gene expression analysis. *Nat. Protoc.* **2**, 1565–1572 (2007).
61. L. Wang, H. Chen, C. Wang, Z. Hu, S. Yan, Negative regulator of E2F transcription factors links cell cycle checkpoint and DNA damage repair. *Proc. Natl. Acad. Sci. U.S.A.* **115**, E3837–E3845 (2018).
62. L. Zhao, L. Xie, Q. Zhang, W. Ouyang, L. Deng, P. Guan, M. Ma, Y. Li, Y. Zhang, Q. Xiao, J. Zhang, H. Li, S. Wang, J. Man, Z. Cao, Q. Zhang, Q. Zhang, G. Li, X. Li, Integrative analysis of reference epigenomes in 20 rice varieties. *Nat. Commun.* **11**, 2658 (2020).
63. L. Wang, L. Zhan, Y. Zhao, Y. Huang, C. Wu, T. Pan, Q. Qin, Y. Xu, Z. Deng, J. Li, H. Hu, S. Xue, S. Yan, The ATR-WEE1 kinase module inhibits the MAC complex to regulate replication stress response. *Nucleic Acids Res.* **49**, 1411–1425 (2021).
64. T. Pan, S. Gao, X. Cui, L. Wang, S. Yan, APC/CCDC20 targets SCFFBL17 to activate replication stress responses in Arabidopsis. *Plant Cell* **35**, 910–923 (2023).

Acknowledgments: We are grateful to Y. Ding for providing the *vip5-2* mutant, Q. Chen for helpful discussion, and M. Shi for sequencing data analysis. **Funding:** This work was supported by the National Key Research and Development Program of China (2023YFF1001300), the National Natural Science Foundation of China 32270306. the National Natural Science Foundation of China 32070312, and the HZAU-AGIS Cooperation Fund SZYJY2022004. **Author contributions:** Conceptualization: S.Y., Y.G., and C.L. Methodology: Y.G., C.L., and H.M. Investigation: Y.G., C.L., Y.L., and YZ. Visualization: C.L. Supervision: S.Y. and L.W. Writing—original draft: Y.G. and S.Y. Writing—review and editing: Y.G., S.Y., C.L., L.W., and P.G. **Competing interests:** The authors declare that they have no competing interests. **Data and materials availability:** Raw sequence data reported in this paper have been deposited in the Genome Sequence Archive in National Genomics Data Center China National Center for Bioinformation/Beijing Institute of Genomics, Chinese Academy of Sciences (https://ngdc.cncb.ac.cn/gsa) with the following accession numbers CRA027026, CRA024642, and CRA024648. All other data needed to evaluate the conclusions in the paper are present in the paper and/or the Supplementary Materials.

Submitted 28 April 2025
Accepted 26 August 2025
Published 26 September 2025
10.1126/sciadv.ady5876